EUROFUSION WPBB-CP(16) 15050

S. Ruck et al.

Thermal Performance Augmentation by Detached Rib-Arrays for Helium Gas Cooled First Wall Applications

Preprint of Paper to be submitted for publication in Proceedings of 29th Symposium on Fusion Technology (SOFT 2016)

This work has been carried out within the framework of the EUROfusion Consortium and has received funding from the Euratom research and training programme 2014-2018 under grant agreement No 633053. The views and opinions expressed herein do not necessarily reflect those of the European Commission.

Thermal performance augmentation by rib-arrays for helium-gas cooled First Wall applications

Sebastian Ruck, Benedikt Kaiser, Frederik Arbeiter

Karlsruhe Institute of Technology, Institute of Neutron Physics and Reactor Technology, Eggenstein-Leopoldshafen, Germany

Rib-roughening the helium-gas cooled channels in the plasma facing components of DEMO (First Wall, limiters or the divertor) enhances heat transfer and reduces structural material temperatures. The present study examines the applicability of six different attached rib-arrays and of two different detached rib-arrays for increasing the thermal performance within the helium-gas First Wall cooling concept. The rib-arrays consist of transversally oriented or 60 deg. (with respect to the centerline) V-shape rib-elements with different rib-element cross-section (square, trapezoid, 2 mm radius round-edged front- and rear-rib-surface). Turbulent flow and heat transfer for 8 MPa pressurized helium-gas with a helium mass flow rate of 0.049 kg/s were computed by Detached-Eddy-Simulations. A constant heat flux density of 0.75 MW/m^2 and 0.08 MW/m^2 respectively was applied at the plasma-facing and breeding-blanket-facing First Wall structural surface. The results show that structuring the thermally highly loaded cooling channel surface by 60 deg. V-shape rib-elements provides an efficient heat transfer, increases the cooling performance and the structural temperature of the First Wall maintains below the structural temperature upper limit of 550 °C.

Keywords: First Wall Cooling, Helium Gas, Structured Cooling Channels, Rib-Arrays, Detached Eddy Simulation.

1. Introduction

Pressurized helium-gas is a coolant in several breeding blanket (BB) design concepts of the DEMO fusion power reactor. Compared to water and liquid metals, helium is inert for chemical and nuclear reactions, causes no corrosion or activation and offers a wide temperature range for cooling without phase transformation. Improved designs of the First Wall (FW) cooling channels (CC) with rib-roughened or structured CC surfaces enhances the heat transfer and can compensate the comparable low volumetric heat capacity and thermal conductivity of helium-gas. The rib-elements placed at the thermally highly loaded CC surface induce a three-dimensional, unsteady flow field and heat transfer is augmented by mixing the fluid in the near wall regions and boundary layers providing a reduction of the maximum FW structural temperature and a raise in the mean coolant temperature [1]. Both effects increase the functionality of the FW cooling performance and can raise the degree of efficiency of the primary heat transfer system and balance of plant. Unfortunately, the rib-elements increase the flow resistance, and thus, the pumping power is raised [2]. Furthermore, the manufacturing of rib-roughened CC surface is complex. However, the disadvantages due to increased pumping power and complex manufacturing can be small compared to the benefits of the enhanced heat transfer, e.g. increased component life time or load flexibility. Flow and temperature fields of attached rib-arrays have been investigated extensively for decades [3-5]. The applicability of rib-roughened CC for helium-gas cooled FW applications and their prospects of success in efficiency and effectiveness were depicted by Ruck and Arbeiter 2016 [1], Arbeiter et al. 2016 [6] and Chen and Arbeiter 2015 [7].

The objectives of the present study are to evaluate the pressure drop, heat transfer coefficients, temperatures and the efficiency of FW CC structured by several rib-array configurations. The presented CC designs are studied for the ‘integrated’ FW concept, but can be adopted to the ‘de-coupled’ FW concept too.

2. Numerical Methods

2.1 Computational Domain

Flow and conjugated heat transfer were computed for an unscaled section of the FW of DEMO including the solid structure and fluid domain as shown in Fig. 1. The FW thickness was 30 mm, the channel cross section was 15 mm x 15 mm with an inner radius of 2 mm or 90 deg. edges, the rib-height was e = 1 mm, the rib-pitch-to-rib-height-ratio was p/e = 10 and the rib-height-to-hydraulic-diameter-ratio was e/D_h = 0.0653 and 0.0638 (depending on the rib-array). The plasma-facing CC surface was structured by (A) attached rib-arrays and (D) detached rib-arrays of 18 centrally positioned, (T) transversally oriented rib-elements or (V) 60 deg. V-shape rib-elements with different rib-element cross-sections ((1) square, (2) 2 mm radius round-edged front- and rear-rib-surface, (3) trapezoid). For the detached rib-arrays the clearance to the channel wall was c = 0.1 mm. The length of the computational domain was 180 mm. The rib-array configurations are sketched in Fig. 2.

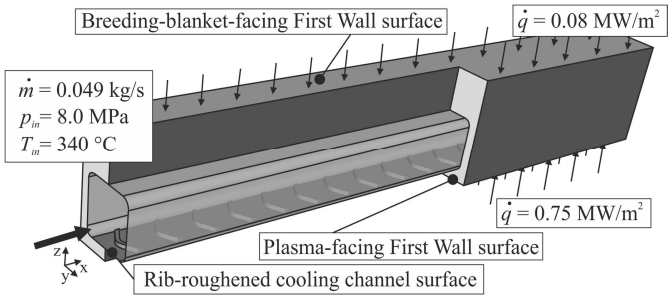

Fig. 1. Computational domain of the First Wall cooling channels.

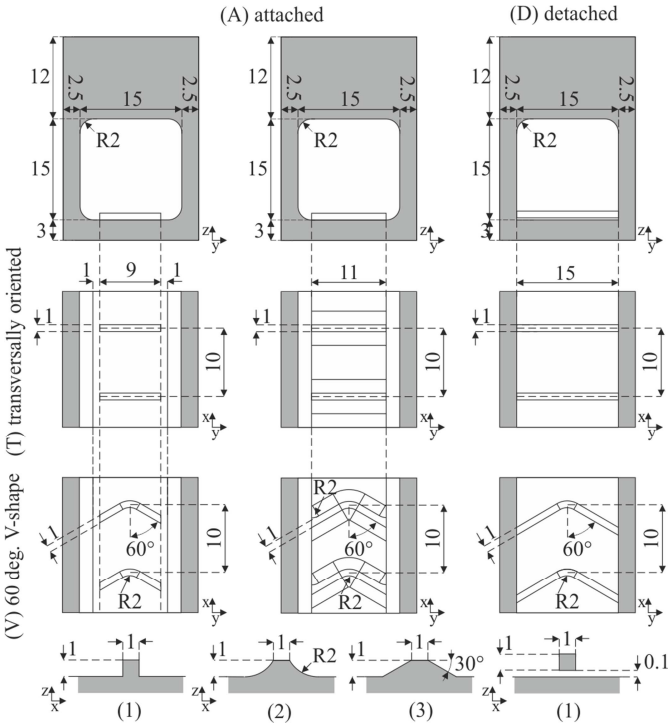

Fig. 2. Rib-array configurations for the First Wall cooling channels. All dimensions are given in mm.

2.2 Simulation Details and Boundary Conditions

Turbulent flow and heat transfer were computed by the delayed Detached-Eddy-Simulation (DDES) approach. The commercial finite-volume-method solver FLUENT V.15 [8] was used. Details of the applied algorithm and discretization schemes are described in Ruck and Arbeiter 2016 [2]. The computations were conducted for pressurized helium-gas with a mass flow rate of $\dot{m}$ = 0.049 kg/s (corresponding to a Reynolds number of Re = $1.05 \cdot 10^5$ based on the hydraulic diameter D_h), with an inlet pressure of p_{in} = 8 MPa(abs) and with an inlet temperature of T_{in} = 340 °C. Ideal gas conditions with temperature dependent specific heat capacity c_p^{He}, thermal conductivity k^{He} and fluid viscosity ν^{He} [9] were assumed. The baseline structural material for the FW is EUROFER steel [10]. The specific heat capacity c_p^{E} [11] and thermal conductivity k^{E} [12] were temperature dependent parameters, while an averaged density of ρ^{E} = 7620 kg/m^3 was applied within the expected temperature range. Symmetry conditions were employed at the outer side, rear and front walls of the solid domain and a constant heat flux density of 0.75 MW/m^2 and 0.08 MW/m^2 respectively were applied at the plasma-facing and breeding-blanket FW surface, see Fig. 1.

The inlet flow was fully turbulent developed. The corresponding velocity profile was obtained separately by isothermal, transient DDES flow simulations in smooth CC with identical geometrical dimensions as the structured CC. Simulations were transient with a CFL number < 1.0. Time-averaging of the results were carried out, after a computationally developed state was reached, for a time period of fifty flow-throughs over one rib-pitch-section.

The mesh size varied for the different rib-configurations in the range from $13.8 \cdot 10^6$ to $20.1 \cdot 10^6$ cells. Local grid refinement was performed in the vicinity of the rib-elements and within the inter-rib-spacing resulting in a focus region with maximum cells sizes of $\Delta x^+ \approx 36$ (streamswise) and $\Delta y^+ \approx \Delta z^+ \approx 25$ (crosswise) and a wall-normal first spacing of $\Delta z^+ < 1$. Numerical uncertainty has been verified by the grid convergence index method as indicated by Roache 1994 [13] and recommended for CFD Studies [14].

2.3 Manufacturing Concepts

The design of the structured FW CC depends on different manufacturing strategies, currently considered for the helium cooled FW. The presented design of the attached rib-arrays bases on the manufacturing strategy of fabricating the FW from two separate shells with the intersection plane at the channel symmetry plane and joining the upper and lower shell by the HIP technique [15]. The CC and the attached rib-arrays are designed for a generation of usual machining of mill cutting with round and spherical head cutters.

For generation the detached rib-arrays, ladder-like tapes of rib-elements can be inserted into support notches located at the CC side walls. The CC (including the support notches) are fabricated by wire cutting of electrical discharge machining [16]. The concept of inserting ladder-like tapes can be adopted for the design and fabrication of the attached rib-arrays by generating two support notches into the CC bottom. Both concepts of ladder-like tape insertion manufacturing are sketched in Fig. 3. Compared to concepts with the die sink erosion techniques for generating rib-roughened CC surfaces within the wire-cut CC manufacturing concept [16], a cost reduction for producing the rib-roughened CC surfaces per linear meter is expected to be in the range of two orders of magnitude by the ladder-like tape insertion manufacturing.

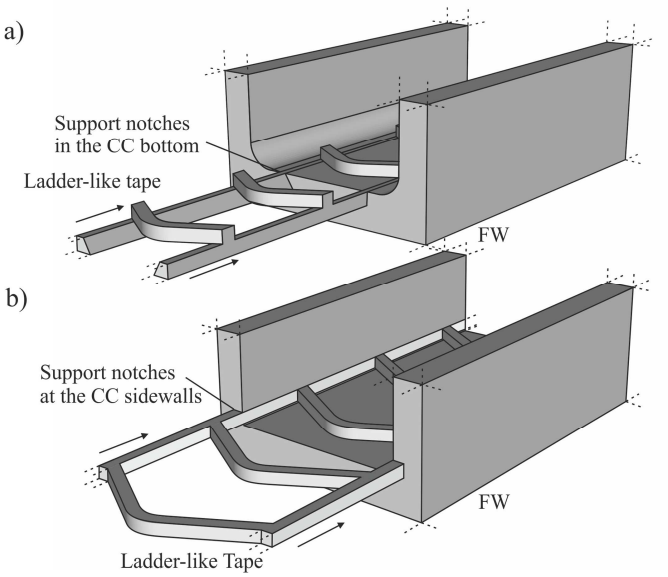

Fig. 3. Ladder-like manufacturing concepts for a. attached rib-arrays and b. detached rib-arrays.

To improve the fitting and to ensure a fixation of the ladder-like rib-array, structural materials with a higher thermal expansion than the FW structural material can be considered for the rib-elements. Small gaps in the order of common manufacturing tolerance occurring between the rib-roughened CC surface and the rib-element will not reduce the functionality of cooling the FW compared to fully attached rib-elements, but can raise the required pumping power [17].

3. Results

2.1 Temperature Distributions

The temperatures in the EUROFER structure and the helium coolant are dominated by the cooling performance of the CC, the rib-array configuration and the thermal heat loads. Maximum temperatures occur at the plasma-facing FW surface. Distributions of mean temperatures $\bar{T}$ and maximum temperatures $\hat{T}$ at the plasma-facing FW surface and at the rib-roughened CC surface with the AT1, AV1 and DV1 rib-array along the CC are shown in Fig 4, representing the characteristics of attached transversally oriented, attached V-shaped and detached V-shaped rib-array(s). For all rib-arrays, coolant bulk temperatures $\bar{T}_b$ increase linearly and a fully thermal-hydraulically developed state was reached after the 9^{th} and 10^{th} rib-element respectively.

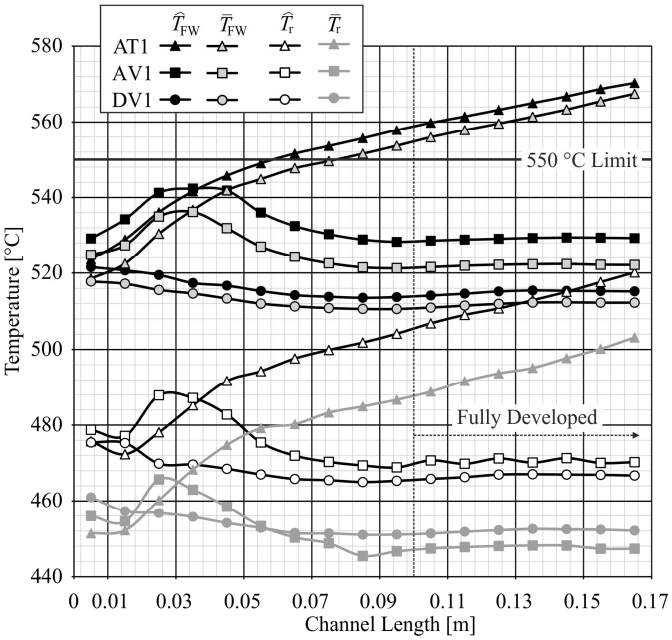

Fig. 4. Mean and maximum temperatures at the plasma-facing FW surface ($\hat{T}_{FW}$, $\bar{T}_{FW}$) and the rib-roughened CC surface ($\hat{T}_r, \bar{T}_r$).

For the CC with the AT1 rib-array, the steep raise of the mean and maximum temperatures within the flow entrance region develops to a linear increase after the 8th rib-element. The extrapolated temperature gradients are 185 °C/m at the plasma-facing FW surface and 220 °C/m at the rib-roughened CC surface along the CC. Temperatures in the EUROFER structure exceed the upper limit of 550 °C [10] within the flow entrance region between the 5th and 7th rib-element.

Temperature profiles of the CC with the AV1 and DV1 rib-array differ within the entrance region. Whereas local peak values occur for the AV1 rib-array, temperatures decrease for the DV1 rib-array. Mean and maximum temperatures of both V-shape rib-arrays remain nearly constant along the CC within the fully developed region: Maximum temperatures at the plasma-facing FW surface are in the range of $\hat{T}_{FW}$ = 528.8 - 529.6 °C for AV1 and in the range of $\hat{T}_{FW}$ = 514.6 - 515.4 °C for DV1. $\hat{T}_{FW}$ increases slightly with temperature gradients of 16.1 °C/m for the AV1 rib-array and 19.8 °C/m for the DV1 rib-array.

2.2 Heat Transfer Coefficient and Pressure Drop

The local distributions of the heat flux densities at the rib-roughened CC surface vary along the CC. The heat transfer coefficient, spatially averaged over each pitch-rib-section area of the rib-roughened CC surface within the fully thermal-hydraulically developed region,

$$\bar{h}_r = \bar{q}_r/(\bar{T}_r - \bar{T}_b) \quad (1)$$

and the corresponding mean axial pressure drop *dp*/*dx* along the CC are shown in Fig. 5, with the spatially averaged coolant bulk temperature $\bar{T}_b$, heat flux density $\bar{q}_r$ and wall temperature $\bar{T}_r$ for each corresponding pitch-rib-section. For the transversally oriented and V-shape attached rib-arrays, the heat transfer coefficients increase in the order of the rib-element cross-section: trapezoid, 2 mm radius round-edged front- and rear-rib-surface and square. The pressure drop is reduced for the trapezoid cross-section and in a comparable range for the remaining ones. The varying pressure drop and heat transfer coefficients are attributed to thermal-hydraulic effects caused by the different cross-sections [2]. The simulation results show that the flow moves smoother over the rib-arrays with trapezoid cross-section than over the square cross-section and, thus, flow acceleration and deceleration decrease and the

pressure and velocity gradients were reduced and smoothed. Furthermore, compared to the square rib-element cross-section, the heat transfer area is reduced for the rib-elements with the 2 mm radius round-edged front- and rear-rib-surface and trapezoid cross-section. The increased pressure drops of the detached rib-arrays are partly attributed to the increased form drag due to the enlarged transversal cross-sectional area and the development of flow stagnation regions at the conjunction of the rib-elements and the sidewalls, accompanied by a decrease of momentum transport and pressure penalty. Additionally, effects of the gap flow and wall-jet flow beneath the rib-elements slightly raise the pressure drop as indicated by Liou et al. 1995 [17].

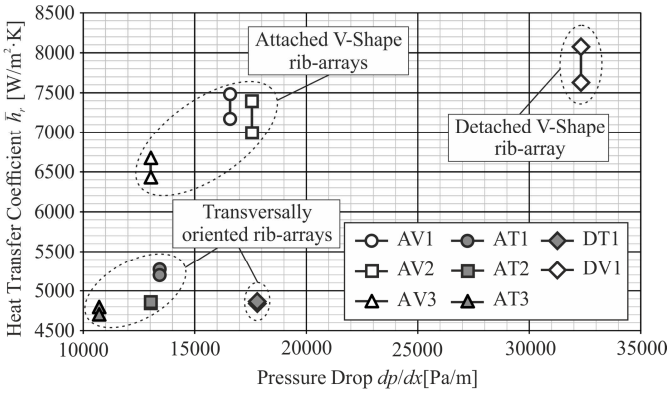

Fig. 5. Heat transfer coefficient and pressure drop with the fully thermal-hydraulically develop region.

Compared to the transversally oriented rib-arrays the pressure drop and heat transfer coefficient of the V-shape rib-arrays are increased. The V-shape configuration causes stronger secondary flow structures in crosswise direction. Vertical flow velocities are up to 4 times higher than for the transversally oriented rib-arrays. Thus, the mixing between the 'hot' wall boundary layer flows and the 'cold' core flow is intensified and heat transfer enhancement at the rib-roughened CC surface and at the sidewalls of the CC is significantly increased for the V-shape rib-arrays. However, the intensified secondary flow raises the pressure drop enormously. The heat transfer coefficients of the V-shape rib-arrays increase linearly along the CC within the fully developed region. The highest heat transfer coefficients are obtained for the AV1 and the DV1 rib-array and are in the range of $\bar{h}_r$ = 7170 -7480 W/m^2·K and $\bar{h}_r$ = 7620 – 8080 W/m^2·K respectively. The corresponding heat transfer coefficient gradients along the CC are 4900 W/m^2·K / m and 6900 W/m^2·K / m. The heat transfer coefficients of the transversally oriented rib-arrays decrease slightly and are in the range of $\bar{h}_r$ = 5270 – 4700 W/m^2·K.

Assuming a steady development of $\bar{T}$ and $\hat{T}$ along the CC, the aforementioned gradients of AV1 and DV1 can be used for temperature and heat transfer estimations in further FW studies.

2.3 Thermal Performance

The thermal performance can be evaluated by comparing the heat transfer coefficient of the rib-roughened CC (h_r) and the heat transfer coefficient of smooth CC (h_0) with equal thermophysical properties φ and characteristic CC lengths l_{ch} for the constraint of equal pumping power $P_r/P_0 = f_r \cdot \dot{m}_r^{\,3} \cdot C(\varphi, l_{ch}, \ldots) / f_0 \cdot \dot{m}_0^{\,3} \cdot C(\varphi, l_{ch}, \ldots) = 1$, with the pumping power P_r and P_0, the friction factor f_r and f_0, the mass flow rate $\dot{m}_r$ and $\dot{m}_0$ and the constant C for the rib-roughened and smooth CC respectively, as recommended by Liou and Hwang 1992 [18]. The friction factor is derived from the pressure drop $f_r = 0.5 \cdot dp/dx \cdot D_h \cdot \rho \cdot A_r \cdot \dot{m}_r^{-2}$, with the CC cross-section A_r. The mass flow rate $\dot{m}_0$ and the heat transfer coefficient h_0 of the smooth CC can be calculated iteratively from the friction factor and Nusselt number correlation of Petukhov and Gnielinski respectively [19]. The ratio h_r/h_0 ($Pr = P_0$) specify the increased heat transfer performance for equal pumping power. On the other side, the thermal performance can be evaluated by comparing the required pumping power of the rib-roughened CC P_r and the smooth CC P_0 for the constraint of equal heat transfer coefficients, $h_r = h_0$. Applying an analogous calculation procedure the ratio P_r/P_0 ($h_r = h_0$) can be evolved, specifying the reduced pumping power for equal heat transfer performance. The ratio h_r/h_0 ($P_r = P_0$) is

potted against the ratio P_r/P_0 ($h_r = h_0$) for the different rib-arrays in Fig. 6. Compared to smooth CC, the pumping power can be significantly reduced to obtain equal heat transfer performance by the use of the presented rib-arrays or, from another point of view, the heat transfer coefficient can be increased with equal pumping power by the use of the presented rib-arrays. Best efficiency was obtained for the AV1 rib-array (highest h_r/h_0 ($P_r = P_0$) and smallest P_r/P_0 ($h_r = h_0$)).

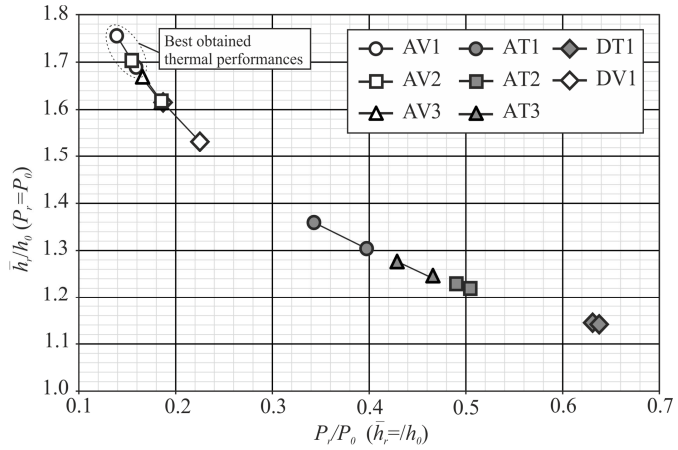

Fig. 6. Thermal Performance

4. Conclusion

The applicability of different rib-arrays for increasing the cooling performance of the helium-gas cooled First Wall cooling channels has been analyzed. It is shown that structuring the thermally highly loaded cooling channel surfaces with optimized rib-arrays provides an efficient heat transfer, increases the cooling performance and reduces structural material temperatures. The main findings are summarized as follows:

(1) Cost-effective manufacturing concepts for generating rib-roughened First Wall cooling channels by the insertion of ladder-like tapes are introduced for the first time. (2) The highest heat transfer coefficients and pressure drops were caused by the detached V-shape rib-array. (3) The V-shape rib-arrays show the best efficiency. (4) The best thermal performance was obtained for the attached V-shape rib-array with square rib-element cross-section. (5) The heat transfer coefficient of the V-shape rib-arrays with square rib-element cross-section provides adequate cooling performance and the temperature of the First Wall maintain below the EUROFER upper limit of 550 °C. (6) Temperature gradients along the CC were evolved from the results and can be used in further studies.

Acknowledgment

This work has been carried out within the framework of the EUROfusion Consortium and has received funding from the Euratom research and training programme 2014-2018 under grant agreement No 633053. The views and opinions expressed herein do not necessarily reflect those of the European Commission.

References

[1] S. Ruck, F. Arbeiter, Thermohydraulics of rib-roughened helium gas running cooling channels for first wall applications, Fusion Engineering and Design 109-111 (A) (2016) 1035-1040.

[2] S. Ruck., F. Arbeiter, Effects of Rib-Configuration on the Thermal-Hydraulics of One-Sided Heated and Rib-Roughened Cooling Channels, HEFAT 12th International Conference on Heat Transfer, Fluid Mechanics and Thermodynamics (2016) 407-412.

[3] G. Rau, M. Cakan, D. Moeller, T. Arts, The Effect of Periodic Ribs on the Local Aerodynamic and Heat Transfer

Performance of a Straight Cooling Channel, *J. Turbomach.*120 (1998) 368-375.
[4] J. C. Han, Heat Transfer and Friction Characteristics in Rectangular Channels With Rib Turbulators, J. Heat Transf. 110 (1988) 321-328.
[5] J. C. Han, Y.M. Zhang, C.P. Lee, Augmented Heat Transfer in Square Channels With Parallel Crossed, and V-Shaped Angled Ribs, J. Heat Transfer 113 (1991) 590-596.
[6] F. Arbeiter, C. Bachmann, Y. Chen, M. Ilić, F. Schwab, B. Sieglin, R. Wenninger, Thermal-hydraulics of helium cooled First Wall channels and scoping investigations on performance improvement by application of ribs and mixing devices, Fusion Engineering and Design (2016) doi:10.1016/j.fusengdes.2016.01.008.
[7] Y. Chen, F. Arbeiter, Optimization of channel for helium cooled DEMO first wall by application of one-sided V-shape ribs, Fusion Engineering and Design 98–99 (2015) 1442–1447.
[8] ANSYS Fluent Theory Guide, Release 15.0 (2013).
[9] VDI, Heat Atlas 2nd ed., Springer-Verlag Berlin Heidelberg (2010).
[10] T. R. Barrett, G. Ellwood, G. Pérez, M. Kovari, M. Fursdon, F. Domptail, S. Kirk, S.C. McIntosh, S. Roberts, S. Zheng, L.V. Boccaccini,J-H. You, C. Bachmann, J. Reiser, M. Rieth, E. Visca, G. Mazzone, F. Arbeiter and P.K. Domalapally, Progress in the Engineering Design and Assessment of the European DEMO First Wall and Divertor Plasma Facing Components, (2016) DOI: 10.1016/j.fusengdes.2016.01.052.
[11] K. Mergia, N. Boukos, Structural, thermal, electrical and magnetic properties of Eurofer 97 steel, Journal of Nuclear Materials 373 (1) 2008 1-8.
[12] CEA DEN-SAC Appendix A – Material Design Limit Data A3.S18E Eurofer Steel, 2004.
[13] P. J. Roache, Perspective: A Method for Uniform Reporting of Grid Refinement Studies, J. Fluids Eng. 116 (3) (1994) 405-413.
[14] Procedure for Estimation and Reporting of Uncertainty Due to Discretization in CFD Applications, J. Fluids Eng. 130 (7) (2008).
[15] H. Neuberger, A. von der Weth, J. Rey, KIT induced activities to support fabrication, assembly and qualification of technology for the HCPB-TBM, Fusion Engineering and Design 86 (9–11) (2011) 2039–2042.
[16] H. Neuberger, J. Rey, A. von der Weth, F. Hernandez, T. Martin, M. Zmitko, A. Felde, R. Niewöhner, F. Krüger, Overview on ITER and DEMO blanket fabrication activities of the KIT INR and related frameworks, Fusion Engineering and Design 96–97 (2015) 315–318.
[17] T.-M. Liou, W.-B. Wang, Y.-J. Chang, Holographic Interferometry Stud of Spatially Periodic heat transfer in a Channel With Ribs Detached From One Wall, J. Heat Transf., 117 (1995) 32-39.
[18] T.-M. Liou, J.-J. Hwang, Developing Heat Transfer and Friction in a Ribbed Rectangular Duct With Flow Separation at Inlet, J. Heat Transf., 114 (1992) 565-573.
[19] F.P. Incropera, D.P. DeWitt, Fundamentals of Heat and Mass Transfer 6th ed., Wiley (2007).